Frontiers of Information Technology & Electronic Engineering
www.jzus.zju.edu.cn; engineering.cae.cn; www.springerlink.com
ISSN 2095-9184 (print); ISSN 2095-9230 (online)
E-mail: jzus@zju.edu.cn

Analysis and design of novel wideband and high efficiency millimeter-wave antenna arrays for 60-GHz applications

Kai-lai WU[1], Yuan YAO[‡1], Xiao-he CHENG[1], Jun-sheng YU[1], Tao YU[2], Xiao-dong CHEN[3]

[1]*Beijing Key Laboratory of Work Safety Intelligent Monitoring, School of Electronic Engineering, Beijing University of Posts and Telecommunications, Beijing 100876, China*

[2]*Department of Electrical and Electronic Engineering, Tokyo Institute of Technology, Tokyo 152-8552, Japan*

[3]*School of Electronic Engineering and Computer Science, Queen Mary University of London, London E1 4NS, UK*

E-mail: {2018010115, yaoy, xiaohec, jsyu}@bupt.edu.cn; yutao@mobile.ee.titech.ac.jp; xiaodong.chen@qmul.ac.uk

Received Sept. 2, 2019; Revision accepted Dec. 30, 2019; Crosschecked Jan. 6, 2020

Abstract: A type of millimeter-wave antenna array with flexible design is proposed for a variety of applications at 60 GHz. The antenna array can be adjusted to be linearly or circularly polarized by simply changing the radiation part of the antenna array. High gain, wideband, and high radiation efficiency characteristics can be achieved by adopting a low insertion loss feeding network and broadband antenna elements. For the linearly polarized antenna array, simulation results show that the impedance bandwidth of the 2×2 antenna subarray reaches 21.6%, while the maximum gain achieves 15.1 dBi and has a fluctuation of less than 0.4 dBi within the working bandwidth. Simulation results of the 8×8 linearly polarized antenna array show a bandwidth of 21.6% and a gain of (26.1±1) dBi with an antenna efficiency of more than 80%. For the 8×8 circularly polarized antenna array, simulation results show that an impedance bandwidth of 18.2% and an axial ratio (AR) bandwidth of 13.3% are obtained. Gain and efficiency of up to 27.6 dBi and 80% are achieved, respectively. A prototype of antenna array is fabricated, and results are compared and analyzed.

Key words: 60 GHz; Antenna array; Linearly polarized; Circularly polarized; Millimeter-wave
https://doi.org/10.1631/FITEE.1900461 **CLC number:** TN82

1 Introduction

Nowadays, due to the continuous development of the 5th generation mobile networks, the millimeter-wave frequency band (mm-waveband) and its applications have drawn much attention. In the mm-waveband, the ultra-low-latency and ultra-high-speed wireless data transmission becomes feasible, because of the ultra-wide available frequency spectrum (Rappaport et al., 2013). Specifically, the unlicensed 60-GHz band (Rappaport et al., 2011), where 7-GHz continuous bandwidth is available, has attracted much attention. However, the high free space loss, blockage effect, and oxygen absorption at 60-GHz band have become great barriers for applications (Parshin et al., 2001). To address the challenges, an antenna with high gain characteristic plays an important role in millimeter-wave communication systems. As one of the conventional candidates, the reflector antenna can provide a stable gain, while the planar antenna arrays are more desirable for their low profile and high efficiency. A low temperature co-fired ceramics (LTCC) based microstrip patch antenna array has been reported (Du et al., 2017). It achieves wide −10-dB $|S_{11}|$ and 3-dB axial ratio (AR) bandwidths of over 29.6% and 26% respectively, and the maximum gain of the four-element array is 9.3 dBi with slight fluctuations over the bandwidth. However, its efficiency is only about 50%, and such a

‡ Corresponding author
ORCID: Kai-lai WU, https://orcid.org/0000-0001-6836-0545; Yuan YAO, https://orcid.org/0000-0003-4408-3031; Xiao-he CHENG, https://orcid.org/0000-0001-9420-778X; Xiao-dong CHEN, https://orcid.org/0000-0002-1972-3271

high loss severely limits its applications in millimeter-wave wireless systems. A microstrip line feeding patch antenna array employing an FR-4 substrate has been proposed (Lee and Yoon, 2017). An impedance bandwidth (VSWR<2) of 22.03% and an AR<3 dB circularly polarized (CP) bandwidth of 18.18% are achieved, but its poor efficiency becomes a barrier to applications. Results of a six-element series-fed antenna array based on substrate integrated waveguide (SIW) and coplanar waveguide (CPW) show that the array has an operating bandwidth of more than 18.2% (55–66 GHz) with a peak gain reaching 20.4 dBi and its aperture efficiency reaches 44.6% (Zhu et al., 2017). A 2×2 antenna array based on CPW has been introduced (Hao and Li, 2017), using the compact magneto-electric dipole as the antenna element. The 10-dB impedance bandwidth of the 2×2 array is 36.6% and a stable gain of (11.6±0.6) dBi is achieved. The corporate feeding structure is introduced and the efficiency of the array significantly rises to around 70%, which is an obvious improvement compared with the antenna array fed by microstrip line. The performances of the antenna array indicate that the feeding network has impacts on the performance of the antenna array, especially in the high-frequency band.

To further improve the gain of the antenna, it would be an effective method to enlarge the size of the array. However, during increasing the number of elements in an antenna array, how to overcome the impedance matching difficulty and prevent the decrease of efficiency would be challenges. An 8×8 antenna array employing a wideband magnetoelectric (ME)-dipole microstrip radiation element based on SIW feeding network has been introduced (Li and Luk, 2016). The measured impedance bandwidth of the fabricated prototype is 18.2% for $|S_{11}|<-10$ dB, and an AR bandwidth of 16.5% can be achieved by this antenna array without the sequential feed. Due to the use of a full-corporate SIW feed network with low insertion loss, a gain up to 26.1 dBic and good radiation efficiency around 70% are obtained. A 16×16 waveguide slot antenna array with a full-metal waveguide structure shows that about 80% antenna efficiency with a gain of more than 32 dBi is achieved (Miura et al., 2011). Thanks to the low-loss full-copper waveguide feeding network, similar works (Tomura et al., 2012; Yamamoto et al., 2014) also achieved high efficiency of about 80%. However, the inherent disadvantages of the waveguide structure limit its bandwidth, and the bandwidth of the 16×16 antenna array is about only 8.3% (Miura et al., 2011).

The gap waveguide is a new type of low-loss transmission line (Kildal et al., 2008; Zaman and Kildal, 2016). So far, several different types of gap waveguides have been reported, such as the ridge gap waveguide (RGWG) (Zarifi et al., 2016), the groove gap waveguide (GGWG) (Ferrando-Rocher et al., 2018), and the inverted microstrip gap waveguide (IMGWG) (Liu et al., 2017). A conventional RGWG based antenna array has been reported (Zarifi et al., 2016), and the measurement results of the 16×16 slots antenna array demonstrate that the reflection coefficient bandwidth ($|S_{11}|<-10$ dB) covering 56–65.7 GHz frequency band is about 16%, and the measured gain is larger than 32.5 dBi over the band. Compared with the previously mentioned hollow-waveguide slot antenna array with the same size, the efficiency of the antenna array decreases to about 70% due to the contactless air gaps between different layers. An 8×8 antenna array introducing microstrip patch based on RGWG (Zarifi et al., 2017) shows that the bandwidth of VSWR<2 is up to 15.5% (57.5–67.2 GHz). The efficiency remains at about 75% and the gain higher than 21.5 dBi is achieved over the operational bandwidth. A slot antenna array based on the IMGWG (Liu et al., 2017) can be regarded as its feeding part when changing conventional RGWG feeding circuit to the IMGWG network. Analysis results show that the antenna has a 16.95% bandwidth covering a 54–64 GHz frequency band. The measured gain of the antenna is more than 28 dBi with the efficiency about 40% covering a 54–64 GHz frequency band. Compared with the works of Zarifi et al. (2016, 2017) and Liu et al. (2017), we can find that the substrate based antenna element has little impact on the efficiency of the whole antenna array. However, it is clear that the antenna efficiency in arrays with a substrate based feeding network degenerates to arrays with a full-metal feeding structure. Otherwise, full-metal gap waveguide based antenna arrays show high antenna efficiency of more than 70% (Zarifi et al., 2016; Akbari et al., 2018; Ferrando-Rocher et al., 2018; Liu et al., 2018).

As aforementioned, it is hard to maintain the antenna efficiency of a full substrate-based antenna

array, especially for an array of large size, which limits its applications in wireless systems. On the other hand, the conventional full metal based antenna arrays, which employ the slot antenna element, are usually limited in working bandwidth. Since the low-loss and high-efficiency feeding network in an antenna array makes many contributions to the overall antenna efficiency, and the substrate-based radiation has little impact on efficiency, it is possible to ensure both wideband and high antenna efficiency by assembling these two parts together (Zarifi et al., 2017). As Irie and Hirokawa (2017) illustrated, the combination of the dielectric layer and the metal planar waveguide structure can maintain a higher efficiency than the full dielectric structure. Because of the full seal structure, the antenna array can achieve high efficiency. However, the antenna array (Irie and Hirokawa, 2017) still suffers from a narrow working bandwidth for the unchanged form of the waveguide slot antenna element.

In this study, to maintain both the wideband and the high efficiency characteristics in a millimeter-wave antenna array, we propose a type of millimeter-wave antenna array with flexible design at 60 GHz. The antenna array can be linearly or circularly polarized by changing only the radiation of the antenna array. The antenna array can be divided into two parts: a low insertion loss transmission network and a wideband radiation network. A full-metal hollow-waveguide feeding network and microstrip radiation network are employed to maintain both the working bandwidth and efficiency in the antenna array. Note that the two parts of the antenna array are fractional and independent; thus, the linear or circular polarization of the antenna array can be realized by changing only the radiation network without adjusting the feeding network. That is to say, two different polarizations are achieved based on only one feeding network. This design can adapt to different situations. Analysis and simulation results demonstrate that both antenna arrays can obtain wide operating bandwidth and high antenna efficiency. A prototype of the antenna array is fabricated and tested, and the measurement results show good agreement with the simulation results.

2 Linearly polarized antenna element design

Fig. 1 shows the geometry of the proposed high radiation efficiency linearly polarized antenna array. The antenna array can be divided into two parts: a full-corporate-feed hollow-waveguide part and a substrate-based radiation part. The feeding planar waveguide structure is composed of several layers, i.e., feeding apertures, feeding circuit, corporate apertures, and cavities. The feeding circuit combines several planar H-junctions and T-junctions, and the substrate layer consists of microstrip antenna patches and substrate integrated cavities (SIC).

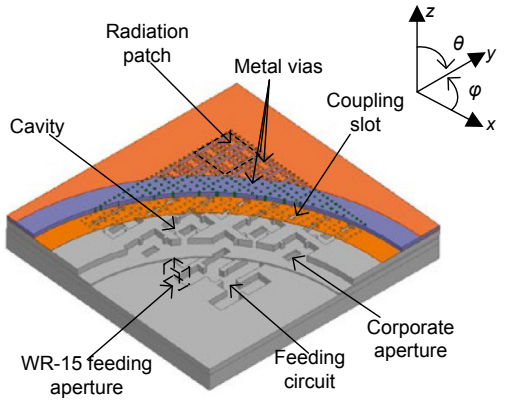

Fig. 1 Linearly polarized antenna array

The whole antenna array is fed by a standard WR-15 waveguide though the aperture in the bottom layer of the feeding circuit. By employing the full-corporate-feed method, low profile and size reduction are realized. The cavities are fed through corporate slots in the lower layer, and the antenna is fed by coupling slots in the bottom metal layer of the substrate. The whole antenna array can be fabricated as follows: the substrate layer with metal covers can be fabricated through a printed circuit board (PCB) process, while the hollow-waveguide feeding part can be realized by several thick-metal layers through the process of diffusion bonding. Then, the two parts can be assembled by screws, making it flexible for different applications.

2.1 Geometry of the antenna element

The three-dimensional (3D) view of the proposed antenna element is shown in Fig. 2. As illustrated in Section 1, the element can be divided into two parts, i.e., the microstrip radiation element and the feeding planar hollow-waveguide. The material of the substrate is Rogers RT/duroid 5880 with relative permittivity ε_r=2.2 and thickness of 0.787 mm. A modified planar microstrip ME-dipole patch (Li and Luk, 2016) is realized by metal vias through the upper

and lower metal layers of the substrate. A substrate integrated cavity (SIC) structure is built by vias and by removing the metal cover around the patch. The detailed geometry of the patch and coupling slots is illustrated in Fig. 3.

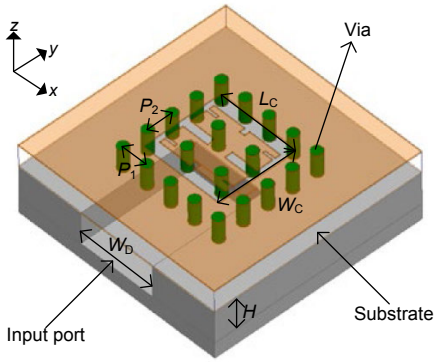

Fig. 2 Three-dimensional (3D) view of the antenna element

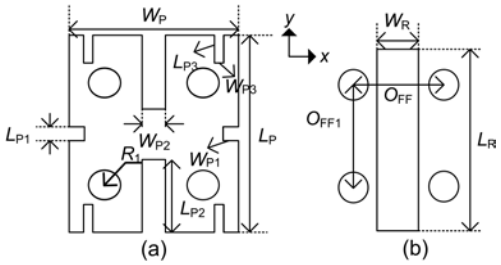

Fig. 3 Detailed geometry of the patch (a) and coupling slots (b)

2.2 Design of the antenna element

The choice of the antenna element plays a crucial role in antenna array design. As illustrated in Fig. 2, the antenna element is combined with a microstrip patch and feeding waveguide; that is, the radiation part in substrate is flexible in the design for relative independence between these two parts. The cut frequency f_c of the planar waveguide can be decided as

$$f_c=\frac{1}{2\sqrt{\mu\varepsilon}}\sqrt{\left(\frac{m}{W_D}\right)^2+\left(\frac{n}{H}\right)^2}, \tag{1}$$

where μ and ε represent magnetic permeability and electric permittivity in air respectively, m=1 and n=0 can be defined by TE_{10} mode, which is the dominant mode of the rectangle waveguide. W_D and H are the width and height of the waveguide, respectively. Then, a suitable dimension can be chosen. To further illustrate the design of the antenna element, three different types of element candidates, i.e., a normal ME-dipole, an ME-dipole with matching slots, and the proposed dipole with slots and cavity are shown in Fig. 4. For comparison with different antenna elements, the dimensions of similar parts of the elements are kept the same. Full wave simulation software Ansoft HFSS is employed to analyze the performance.

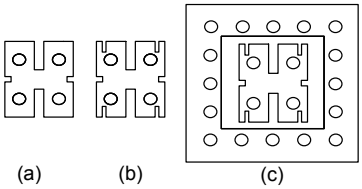

Fig. 4 Three different types of antenna elements: (a) a normal ME-dipole; (b) an ME-dipole with matching slots; (c) the proposed element

The simulation $|S_{11}|$ results of these three types of elements are shown in Fig. 5. Two lines ($|S_{11}|$=−10 dB and −15 dB) are plotted for reference. Compared with the original structure element *A*, element *B* achieves a wide $|S_{11}|$<−10 dB impedance bandwidth covering 55–67 GHz by introducing couples of matching slots. Element *C* reaches the widest $|S_{11}|$<−15 dB bandwidth due to the additional resonance point by the SIC structure, which is beneficial to the radiation pattern and gain performance (Figs. 5b and 5c). It is clear that element *C* can achieve a high and stable gain within the bandwidth thanks to the introduction of the SIC structure. Moreover, the stable gain of element *C* can help reduce the gain loss by reducing the mutual coupling effect between elements when forming the antenna array. In summary, the proposed element performs well as a good candidate for the antenna array.

The microstrip patch with slots can be regarded as a combination of four electric dipoles in the E-plane. The coupling slots in the lower layer work as a couple of equivalent magnetic dipoles in the H-plane through a couple of longitudinal slots in the patch (Hao and Li, 2017). Furthermore, as shown in Fig. 6, at t=0, the surface currents on the patch achieve the maximum intensity and the electric dipoles are excited. At t=T/4 (T represents a period of time), the surface electric field which can be viewed equivalently as magnetic currents is excited and the magnetic dipoles are formed. Although the directions

of currents at $t=T/2$ and $3T/4$ are reverse to those of currents at $t=0$ and $T/4$, the dipoles still work as magnetic dipoles.

2.3 Parameter study of the antenna element

The slots on the antenna element would most affect the impedance and gain performances as previously analyzed. The equivalent magnetic dipoles play a crucial role in the performance of the antenna element. The geometry of the equivalent magnetic dipoles with three different values of W_{P2} and L_{P2} are investigated in Figs. 7 and 8, respectively. The impedance bandwidth of the antenna element is more sensitive to the value of L_{P2}. When increasing the value of L_{P2}, the gain of the antenna element rises, but the amplitude of variation would decrease after certain dimension (Fig. 8). The fluctuation of gain of L_{P2}=1 and 1.2 mm is smaller than that of L_{P2}=0.8 mm. On the other hand, $|S_{11}|$ changes a lot for different values of L_{P2}, and the value of L_{P2} should be chosen properly. The value of W_{P2}, which represents the width of the slots, impacts the impedance

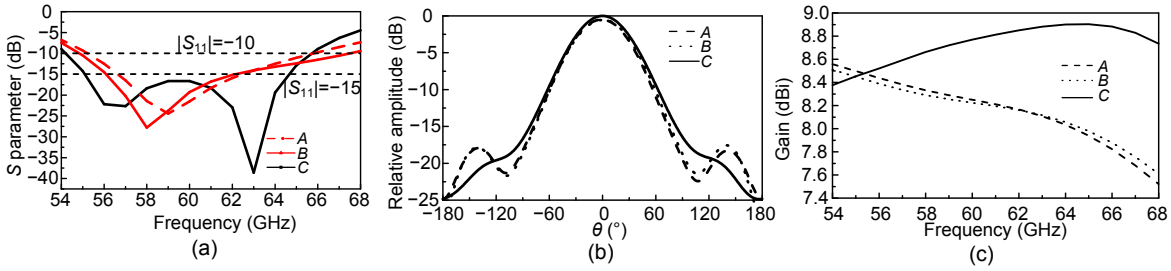

Fig. 5 Simulated $|S_{11}|$ (a), radiation patterns (b), and gain (c) of different types of antenna elements

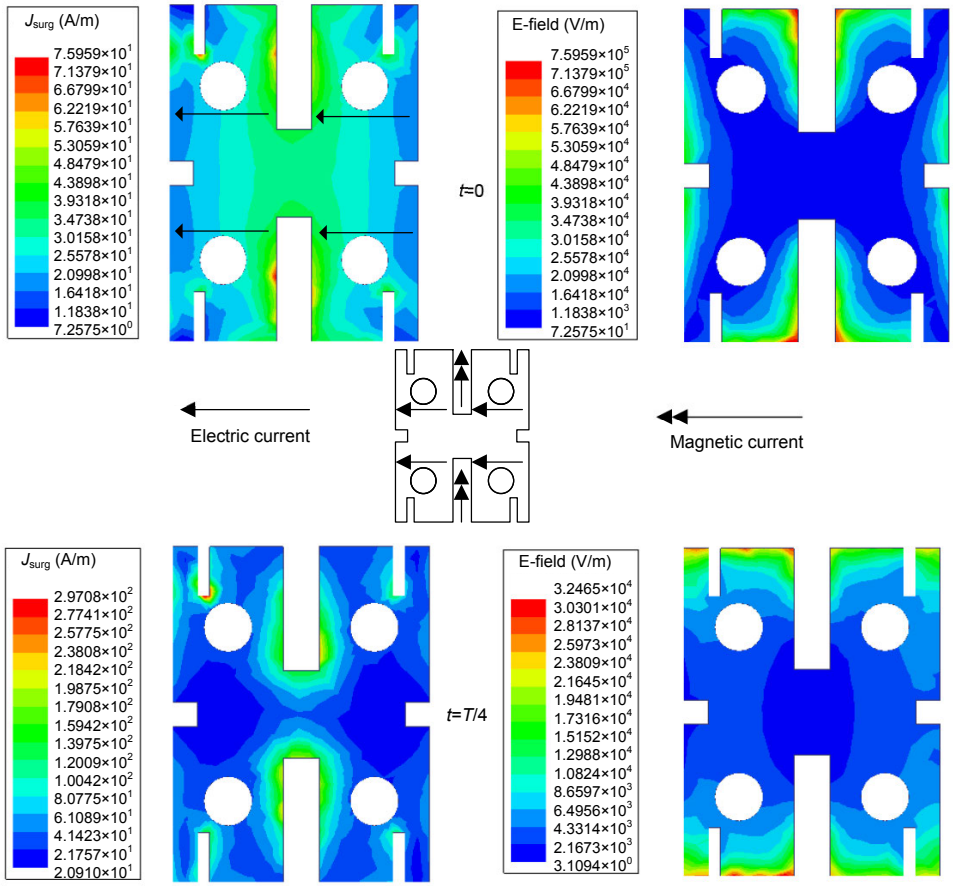

Fig. 6 Current and surface E-field distributions of antenna elements at 60 GHz at different times

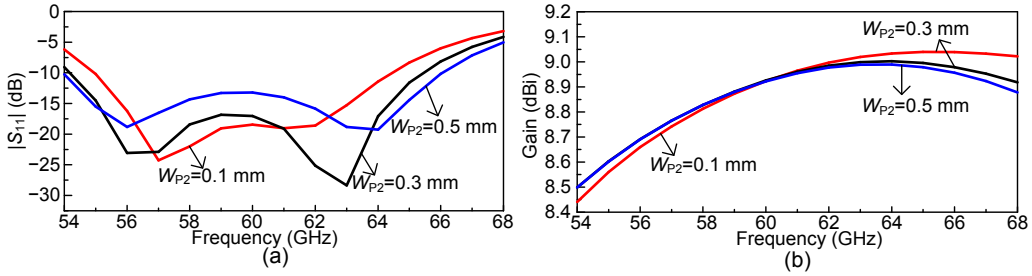

Fig. 7 Simulated $|S_{11}|$ (a) and gain (b) of different values of W_{P2} of the antenna element

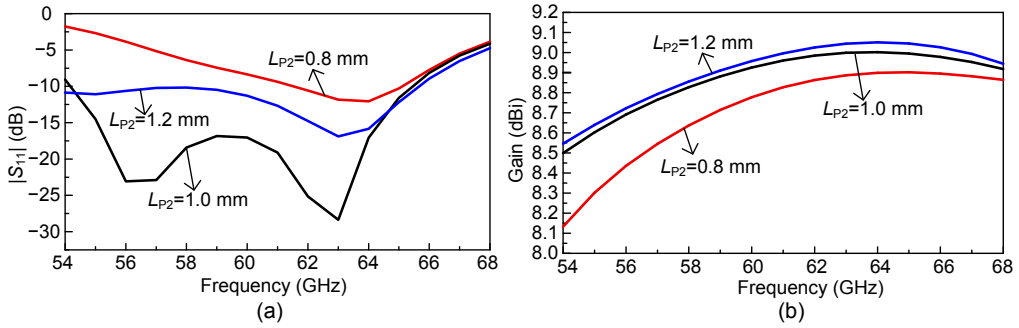

Fig. 8 Simulated $|S_{11}|$ (a) and gain (b) of different values of L_{P2} of the antenna element

performance. Different widths of the slots would change the frequencies of two resonance points when enlarging the value of W_{P2}, and the distance between two resonance points would also be enlarged. However, the gain slightly changes with different values of W_{P2}, meaning that the width of the slots has little influence on the gain performance.

As shown in Figs. 9 and 10, the dimensions of the pair of slots along x-direction are analyzed. The $|S_{11}|$ results indicate that the width and length of the slots almost have no influence on the S parameter performance of the antenna element. The gain results show that the width of the slots would have influence on radiation performance, and this can be employed to tune the element for good performance. The S parameter and gain with different sizes of longitudinal slots of the antenna element are plotted in Figs. 11 and 12. The parameters W_{P3} and L_{P3} represent the width and length of the slots in Fig. 3a, respectively. These two parameters can control the path of surface currents of the antenna element, and then the impedance matching situation would be changed. As shown in Figs. 11a and 12a, the impedance of the antenna element varies with different values of W_{P3} and L_{P3}. Furthermore, the distance between resonance points of the antenna element is changed with different values of W_{P3} and L_{P3}. However, the size of these slots has little impact on the gain of the element (Figs. 11b and 12b).

Figs. 13 and 14 show the influence of different dimensions of the SIC surrounding the antenna element. The W_C in Fig. 2, which represents the width of the cavity, significantly affects the gain of the antenna. The wider cavity achieves the higher gain for more currents along the edge, but the impedance of the element will be different with the changing frequency of resonance points. The length of the cavity L_C impacts the performance of the element in the same way. The enlarging W_C or L_C will clearly increase the gain of the element. However, considering the forming of the antenna array, the distance between elements should be proper for the radiation pattern and to decrease the mutual effects. It means that the overall size of the antenna element should be taken into consideration. Thus, proper W_C and L_C should be chosen.

The design dimensions of the antenna element are listed in Table 1. As shown in Fig. 5a, the antenna element achieves the simulated $|S_{11}|<-10$ dB impedance bandwidth of 19% (54.2–65.7 GHz). The simulated radiation patterns at three frequency points within the bandwidth are plotted in Fig. 15. A simulated gain of (8.6±0.3) dBi with radiation efficiency of more than 97% over the band is obtained (Fig. 16). The cross polarization values are all below −30 dB.

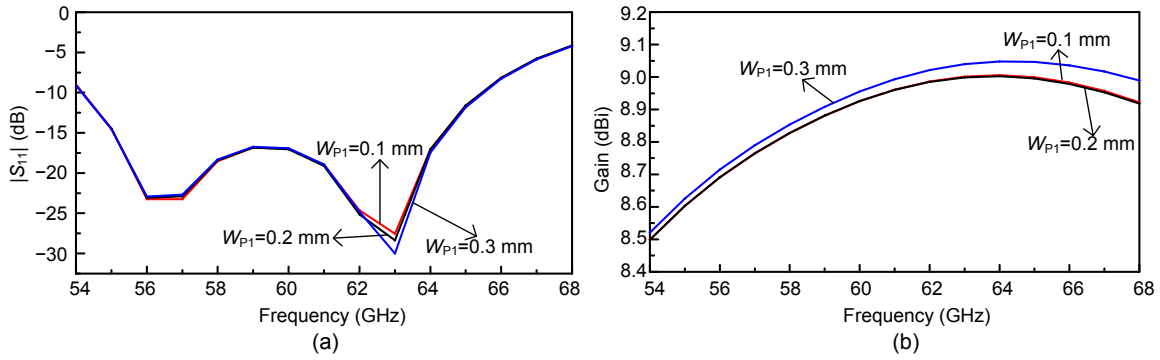

Fig. 9 Simulated $|S_{11}|$ (a) and gain (b) of different values of W_{P1} of the antenna element

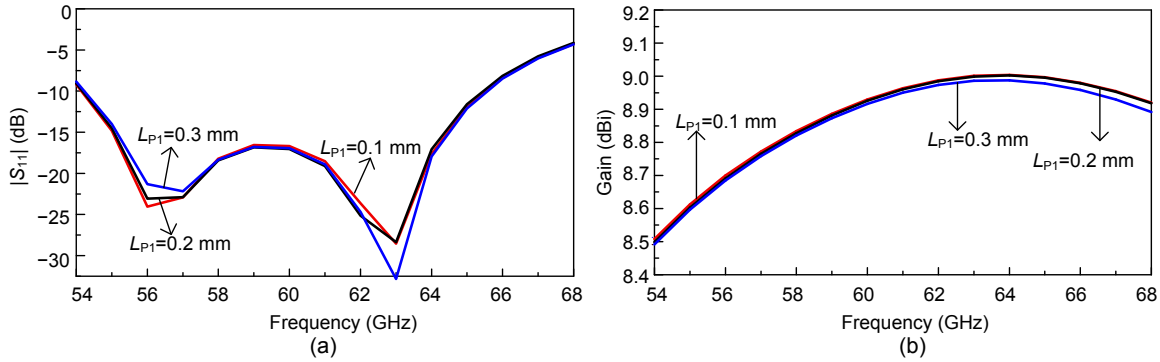

Fig. 10 Simulated $|S_{11}|$ (a) and gain (b) of different values of L_{P1} of the antenna element

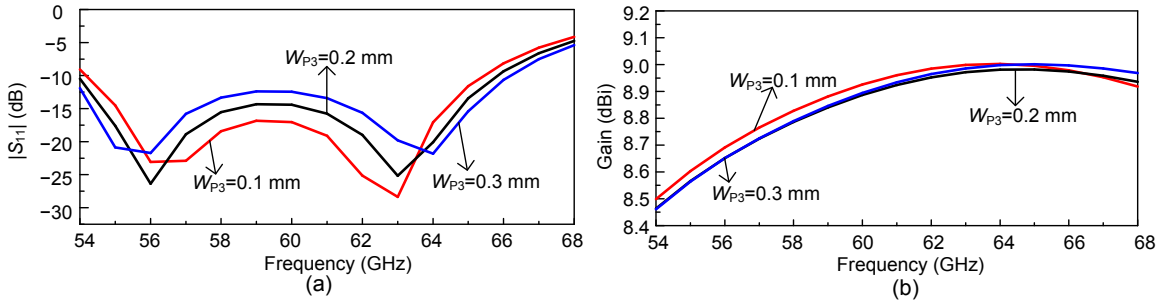

Fig. 11 Simulated $|S_{11}|$ (a) and gain (b) of different values of W_{P3} of the antenna element

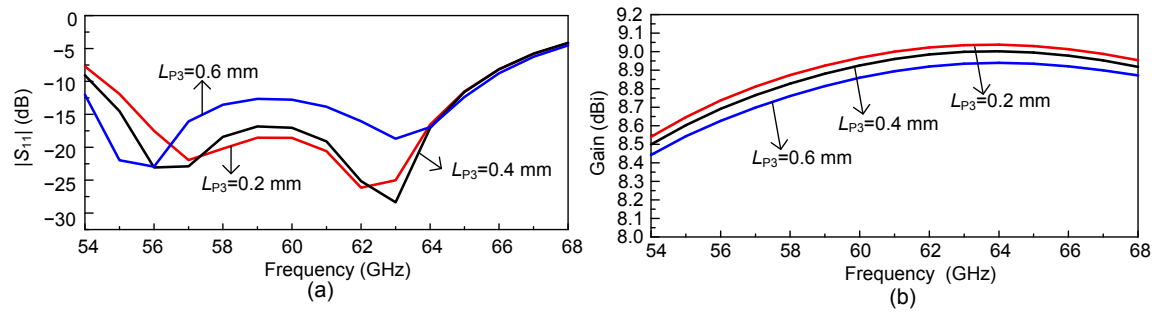

Fig. 12 Simulated $|S_{11}|$ (a) and gain (b) of different values of L_{P3} of the antenna element

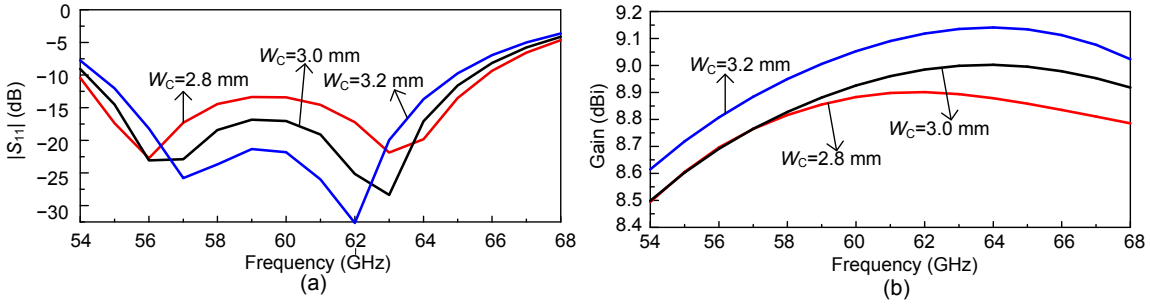

Fig. 13 Simulated $|S_{11}|$ (a) and gain (b) of different values of W_C of the antenna element

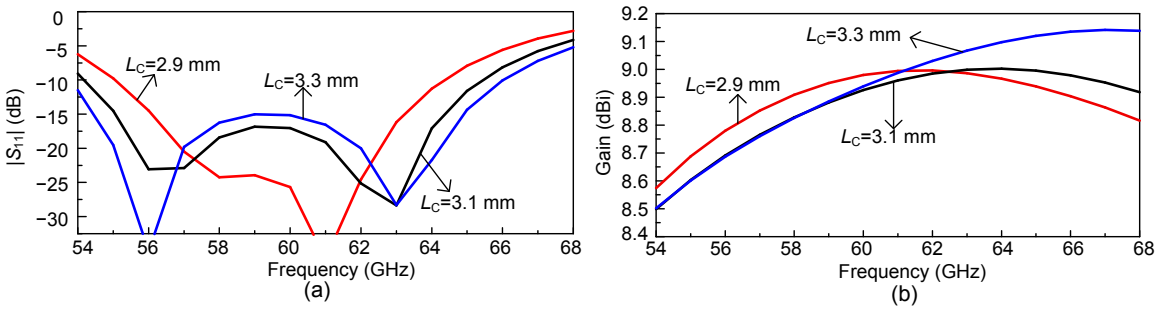

Fig. 14 Simulated $|S_{11}|$ (a) and gain (b) of different values of L_C of the antenna element

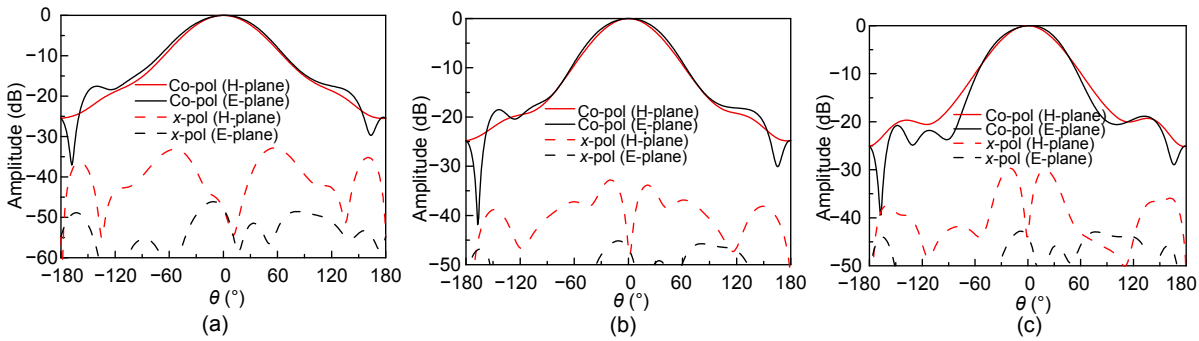

Fig. 15 Simulated radiation patterns of the antenna element at 55 GHz (a), 60 GHz (b), and 65 GHz (c)
Co-pol: co-polarization; *x*-pol: *x*-polarization

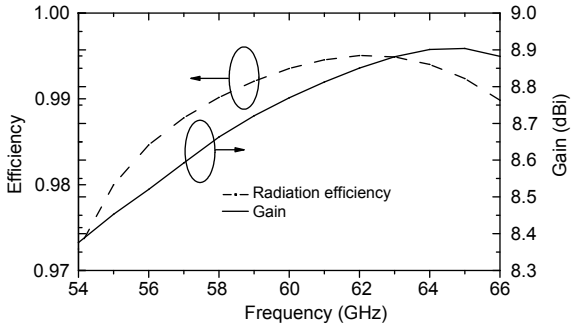

Fig. 16 Simulated gain and radiation efficiency within the bandwidth

Table 1 Antenna element design dimensions

Size	Value (mm)	Size	Value (mm)	Size	Value (mm)
W_D	2.940	W_{P3}	0.100	R_1	0.200
W_P	2.100	L_{P3}	0.400	P_1	0.950
L_P	2.700	W_C	3.000	P_2	0.975
W_{P1}	0.200	L_C	3.100	O_{FF}	1.200
L_{P1}	0.200	H	1.200	O_{FF1}	1.400
W_{P2}	0.300	W_R	0.500		
L_{P2}	1.000	L_R	2.500		

3 Linearly polarized antenna array design

3.1 Design of the proposed 2×2 antenna subarray

A 2×2 antenna subarray based on the proposed antenna element is designed (Fig. 17). It would be regarded as the unit element of the actual 8×8 antenna array, and its performance would be referenced to as that of the actual antenna array. The distance d between the antenna elements in the x and y directions can both be decided as

$$d < \lambda\left(1-\frac{1}{2N}\right), \tag{2}$$

where λ is the wavelength in air and N the number of elements.

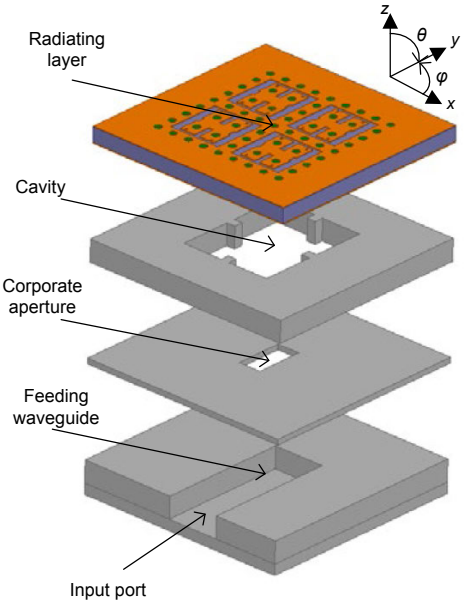

Fig. 17 Configuration of the 2×2 antenna subarray

A cavity with the height of 1.2 mm is added into the subarray to simulate the actual feeding situation, and its detailed geometry is shown in Fig. 18. The design dimensions of the cavity after tuning are listed in Table 2, and the thickness of the corporate aperture is 0.3 mm. The simulated $|S_{11}|$<−10 dB bandwidth reaches 21.6% (54.8–68.1 GHz), and the $|S_{11}|$ keeps below −15 dB (Fig. 19a). The simulated gain and radiation efficiency of the subarray are investigated. A stable gain of (14.7±0.4) dBi and radiation efficiency of more than 90% within the bandwidth are obtained. A suitable element distance is selected and the simulated radiation pattern at 60 GHz shows that a side lobe level (SLL) of about −15dB is realized (Fig. 19b). The simulated cross polarization value is below −43 dB.

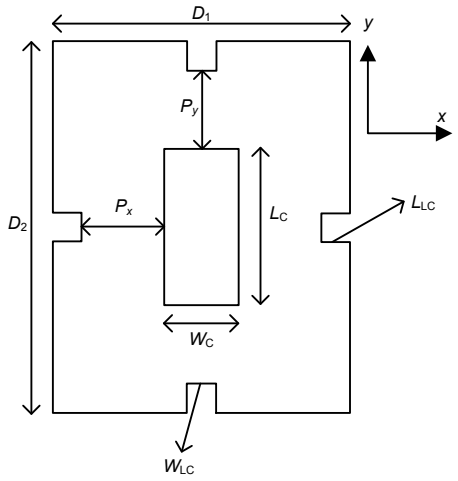

Fig. 18 Detailed geometry of the cavity

Table 2 Dimensions of the cavity design

Parameter	Value (mm)	Parameter	Value (mm)
D_1	3.80	W_C	1.30
D_2	3.90	L_C	2.70
P_x	1.45	W_{LC}	0.50
P_y	1.40	L_{LC}	0.50

3.2 Design of the feeding circuit

One of the crucial parts in the design of the 8×8 antenna array is the feeding circuit. To maintain the performance of the antenna array, stable energy transmission should be ensured. Fig. 20 shows the geometry of the circuit and detailed structures of the H-junction and T-junction. Port 1 represents the WR-15 waveguide input port of the antenna array in Fig. 1, and ports 2–5 represent parts of output ports connecting to the input ports of the antenna subarray. Ports T1–T3 and H1–H5 represent the input ports and output ports of the T-junction and H-junction, respectively. The geometry of the transition of the WR-15 waveguide to the planar waveguide is shown in Fig. 21.

The reflection coefficient and transmission coefficient of T-junction, H-junction, and standard WR-15 waveguide to planar waveguide transition are plotted in Figs. 22, 23, and 24, respectively. In

Fig. 25a, the bandwidth of $|S_{11}|$<−10 dB of the feeding circuit covers the expected bandwidth range of the antenna array (55–68 GHz). *S* parameters of some ports marked in Fig. 20 in the feeding waveguide network of the proposed antenna array are shown in Figs. 25b and 25c. The difference of transmission coefficients of different ports keeps at about 0.1 dB, and the phase difference of different ports is less than 0.6°. A uniform excitation is achieved. Table 3 lists the dimensions of the design presented in Figs. 20 and 21.

3.3 Influence of the additional layer on the 8×8 antenna array

For the fabrication prototype, the substrate board and the waveguide feeding part are assembled by screws along the edges. When two metal surfaces are discontinuous and uneven, the appearance of the air gap due to non-ideal connection is unavoidable. Moreover, the deformation of the substrate layer due to inhomogeneity caused by screws would worsen this issue. The wave leaking formed by the air

Table 3 Dimensions of the power divider design

Parameter	Value (mm)
W_L	2.70
W_{L1}	0.75
L_L	1.10
L_{L1}	0.90
S	0.80

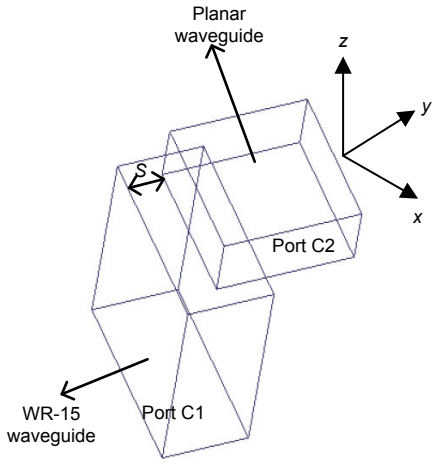

Fig. 21 Detailed geometry of the cavity

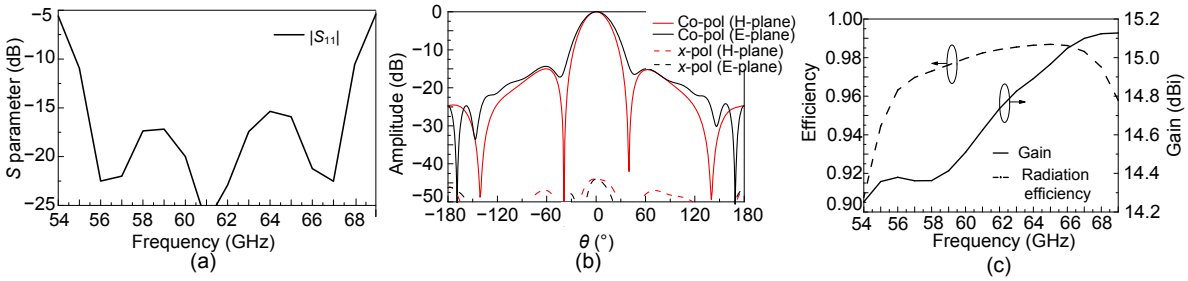

Fig. 19 $|S_{11}|$ (a), radiation pattern at 60 GHz (b), and gain and radiation efficiency (c) of the 2×2 antenna array
Co-pol: co-polarization; *x*-pol: *x*-polarization

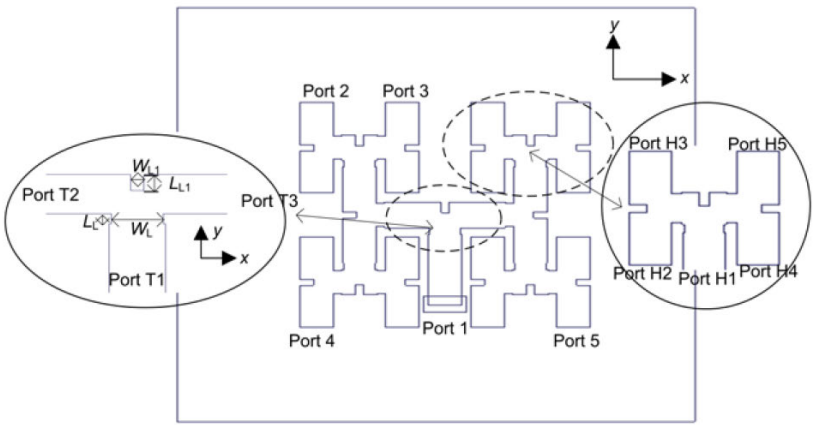

Fig. 20 Geometry of the feeding circuit and detailed structures of the H-junction and T-junction

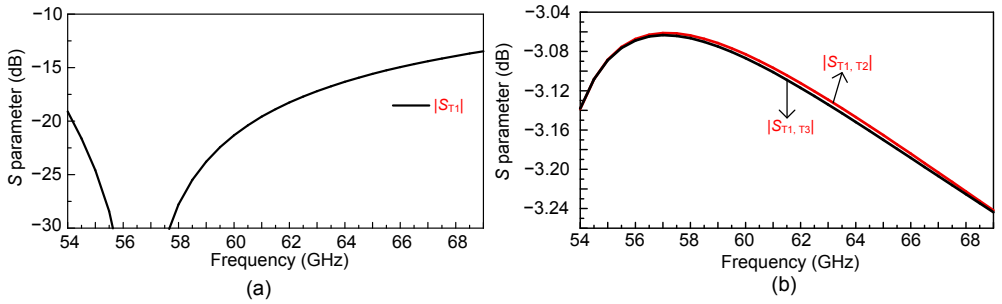

Fig. 22 Simulated *S* parameters of the T-junction: (a) reflection coefficient; (b) transmission coefficient

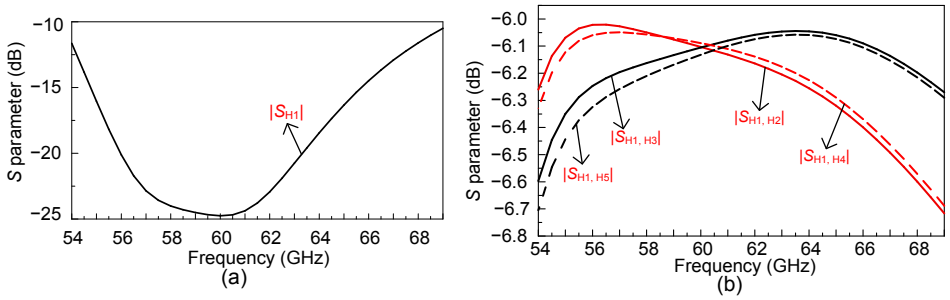

Fig. 23 Simulated *S* parameters of the H-junction: (a) reflection coefficient; (b) transmission coefficient

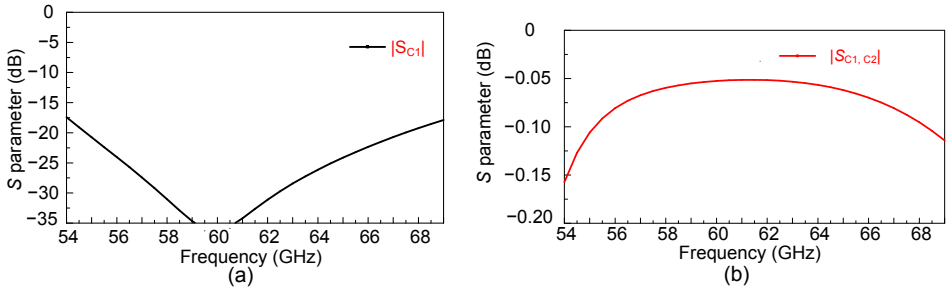

Fig. 24 Simulated *S* parameters of the WR-15 to planar waveguide transition: (a) reflection coefficient; (b) transmission coefficient

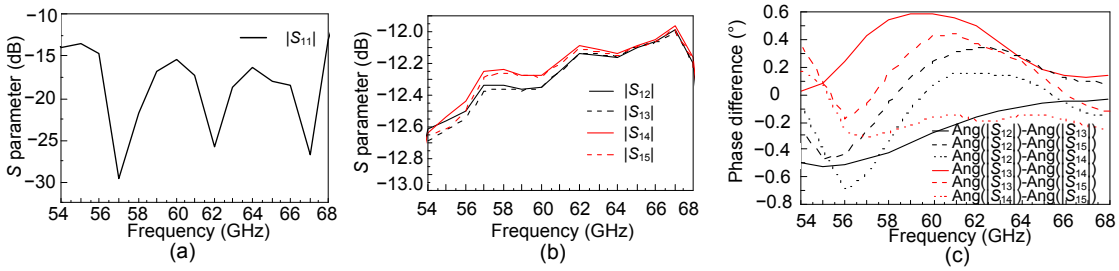

Fig. 25 $|S_{11}|$ (a), transmission coefficient (b), and phase difference (c) of part ports of the feeding circuit

gap would impact the radiation performance and overall antenna efficiency. To lower the impact, an additional layer with thickness of 0.1 mm is added between the cavity layer and the coupling slot layer. The size of slots in the additional layer is larger than that of the coupling slots to avoid mismatching between the two layers, and then the energy would pass through the layer. In the original design, the coupling slots directly connect the cavities, and the cavity would be totally exposed to the air because of the air gap. However, the contact area would be decreased from the area of the cavities to the upper slots

since the introduction of the additional layer, and the issue of wave leaking would be mitigated.

The influence of the additional layer is analyzed in Fig. 26. Figs. 26a and 26c show that the additional layer has little impact on the impedance matching and radiation pattern of the antenna array, respectively. The gain of the antenna array with the additional layer decreases by about 0.8 dBi compared with the array without the additional layer (Fig. 26b), which is acceptable.

4 Circularly polarized antenna array design

The geometry of the proposed 8×8 circularly polarized antenna array is shown in Fig. 27. The substrate layer is replaced with a circularly polarized radiation part compared with Fig. 1, while the geometry of the feeding circuit remains unchanged. Note that an additional layer is added to the feeding circuit as discussed in Section 3.3. The detailed structures of the 2×2 subarray and antenna element are plotted in Fig. 28. The antenna element employs a planar circularly polarized microstrip ME-dipole (Li and Luk, 2016), and the corresponding design parameters are shown in Figs. 28a and 28b.

Fig. 29 illustrates the simulation results of the 2×2 subarray. The simulated $|S_{11}|$<−10 dB bandwidth reaches 15.2% (56.8–66.1 GHz), and AR<3 dB bandwidth of 19.7% (57.2–69.7 GHz). A right-hand circularly polarized gain of up to 15.1 dBic is obtained. The simulated radiation pattern at 60 GHz shows the SLLs at about −14 dB in the *xoz* plane and −17 dB in the *yoz* plane. The design dimensions after tuning are listed in Table 4.

The simulation results of the 8×8 circularly polarized antenna array are shown in Fig. 30. The

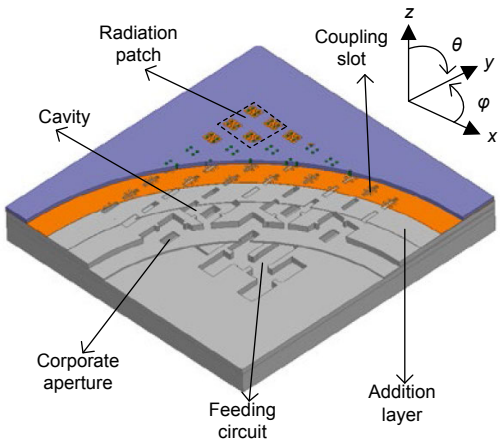

Fig. 27 Configuration of the circularly polarized antenna array

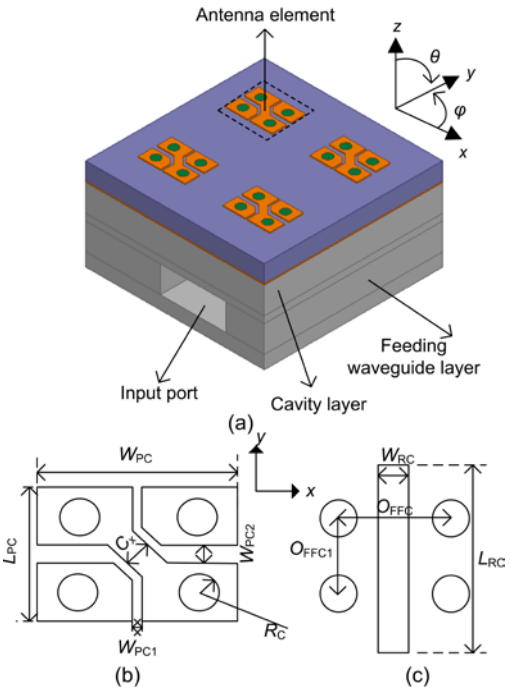

Fig. 28 Configuration of the 2×2 antenna subarray (a), the element patch (b), and its coupling slots (c)

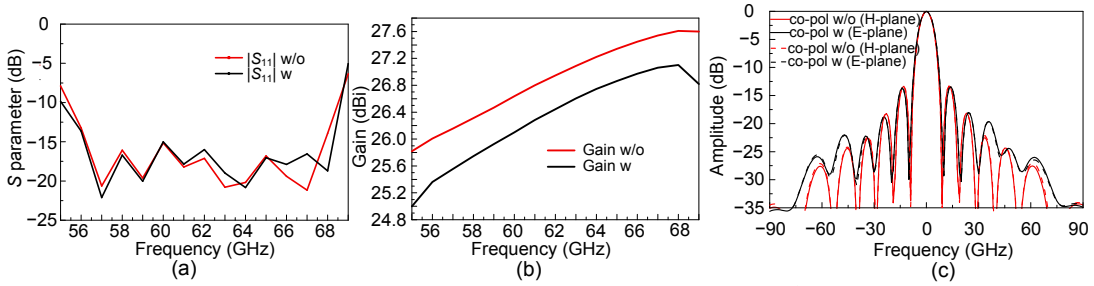

Fig. 26 $|S_{11}|$ (a), gain (b), and radiation pattern (c) of the antenna array without or with the additional layer

w/o and w represent without and with, respectively

impedance bandwidth of 18.2% (56.8–68.1 GHz) and AR bandwidth of 13.3% (56.2–64.2 GHz) are obtained as shown in Figs. 30a and 30b, respectively. The gain of up to 27.6 dBic and efficiency of more than 80% are shown in Figs. 30c and 30d, respectively. Fig. 31 shows the radiation patterns of the 8×8 antenna array at 58, 60, and 62 GHz. The SLLs remain lower than −13 dB and the cross polarization values are below −20 dB at all the three frequencies.

Table 4 Dimensions of the antenna subarray design

Parameter	Value (mm)	Parameter	Value (mm)
W_{PC}	2.10	R_C	0.20
L_{PC}	1.50	O_{FFC}	1.20
W_{PC1}	0.10	O_{FFC1}	0.80
W_{PC2}	0.20	W_{RC}	0.35
C_x	0.20	L_{RC}	2.60

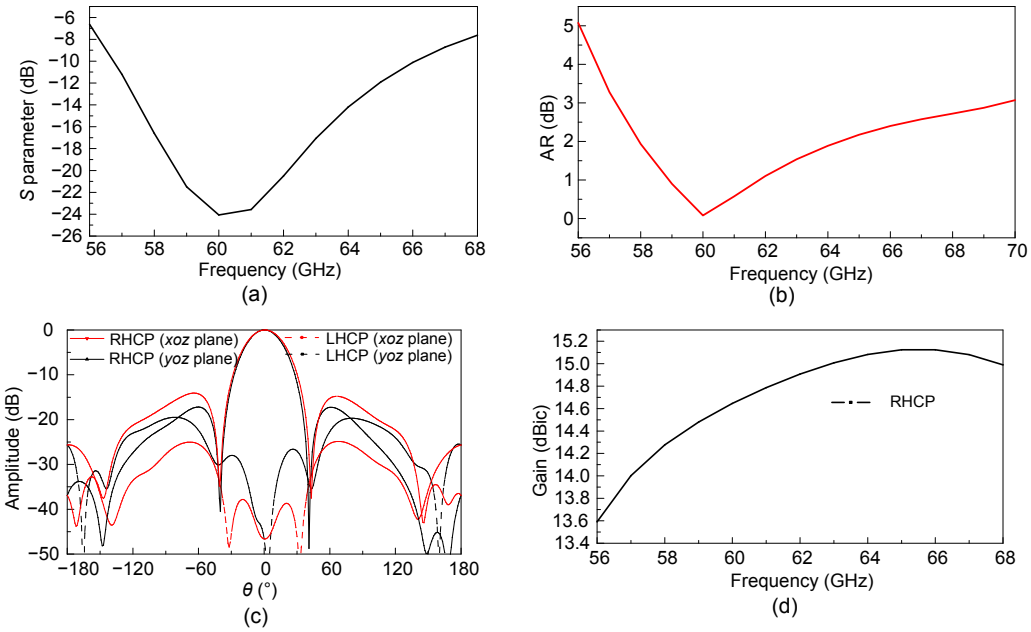

Fig. 29 Simulation results of the antenna subarray: (a) *S* parameter; (b) AR; (c) radiation pattern; (d) gain

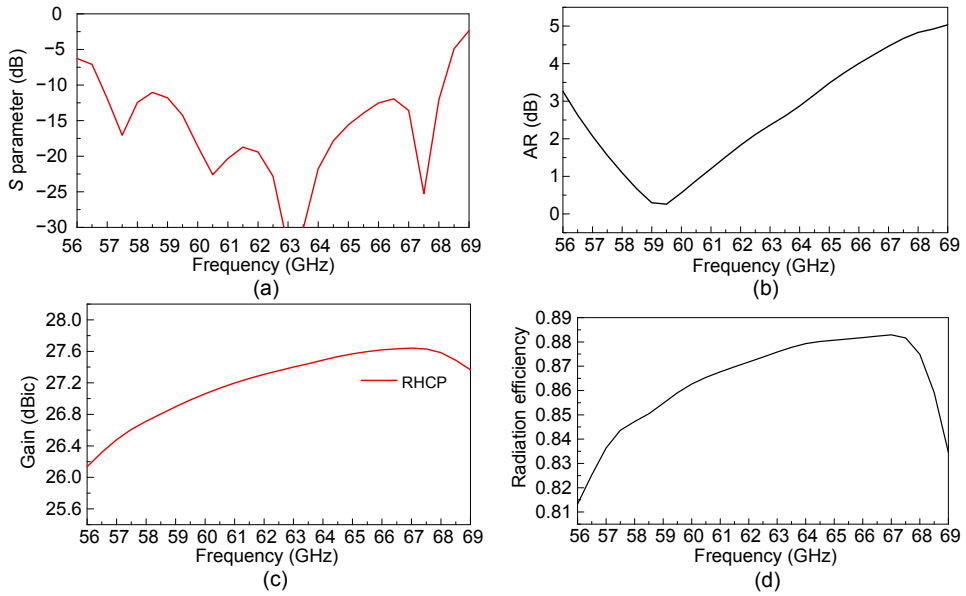

Fig. 30 Simulation results of the 8×8 antenna array: (a) *S* parameter; (b) AR; (c) gain; (d) efficiency

5 Measurement results and analysis

An antenna array prototype is fabricated (Fig. 32). The overall size of the antenna array is 48 mm×46 mm. Note that the assembled prototype is realized by assembling the substrate layer and metal part with screws surrounding the edges of the antenna array, and the surface of the feeding circuit is plated with silver to decrease the conductor loss.

To further illustrate the working principle of the additional layer mentioned in Section 3.3, simulation results of the antenna array with an air gap (thickness of 0.5 mm) between the substrate and waveguide parts are shown in Fig. 33. Fig. 33a shows the simulated and measured $|S_{11}|$ of the antenna array. The measured $|S_{11}|$ has a frequency shift of around 1 GHz compared with the simulated one, and some frequencies in the middle are higher than −10 dB. In Fig. 33b, the measured gain has a decrease within 2 dB compared with the simulated one, and the measured efficiency shows slight decrease, which is within an acceptable range thanks to employing the additional layer. The simulation results with an air gap further indicate the impacts of the wave leaking occurring between the substrate and hollow-waveguide part on the performance of the antenna array. Both the $|S_{11}|$ and the gain show a large decrease due to the appearance of the air gap.

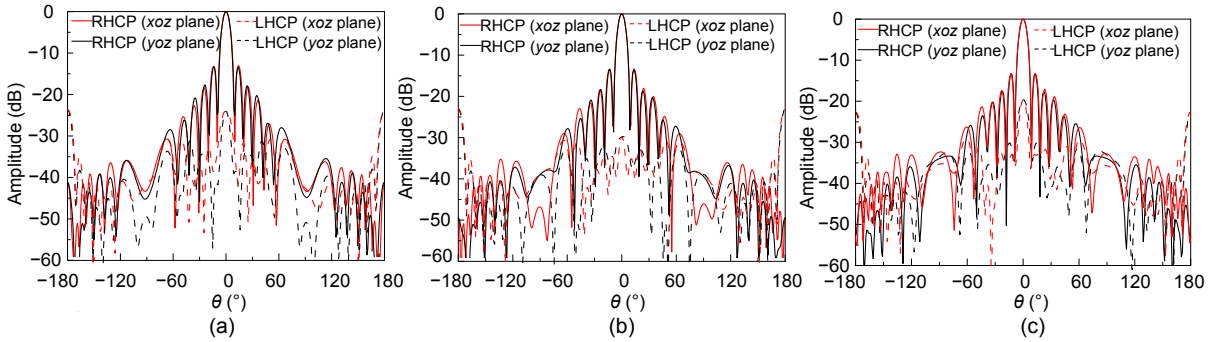

Fig. 31 Simulated radiation patterns of the 8×8 antenna array at 58 GHz (a), 60 GHz (b), and 62 GHz (c)

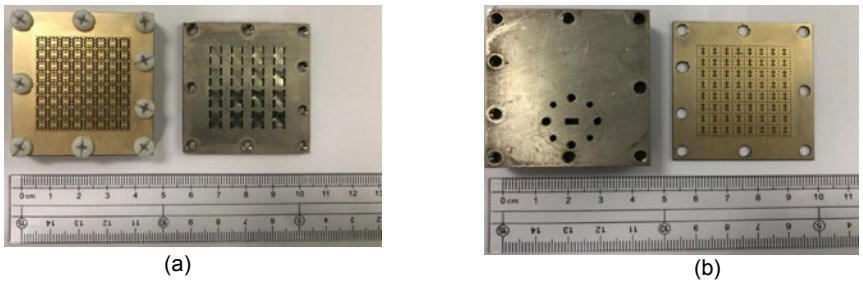

Fig. 32 Fabricated substrate part and hollow-waveguide part prototypes: (a) assembled antenna prototype and the front side of the hollow-waveguide part; (b) the back side of the hollow-waveguide part and substrate part

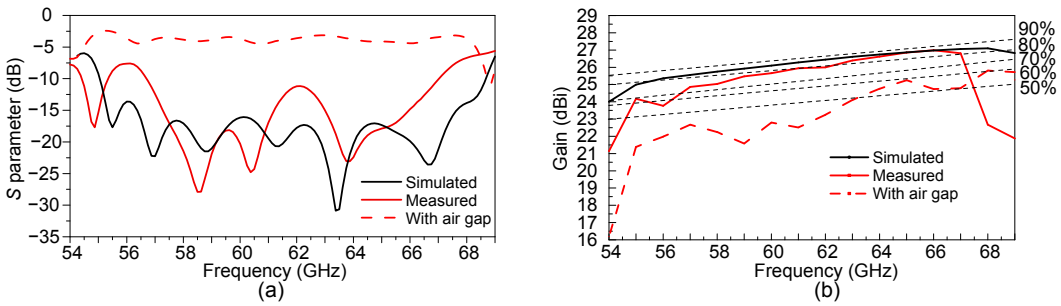

Fig. 33 Simulated and measured $|S_{11}|$ (a) and gain and radiation efficiency (b)

As shown in Fig. 34, the measured cross polarization values are all less than −30 dB at all the three frequency points, which vary by about 20 dB from the simulation values, and the SLLs rise by about 1 dB in the E-plane while almost remaining unchanged in the H-plane. The measured co-polarization shows a great decrease at about θ=−50° (Fig. 34a), which could be caused by the measurement error. Some fundamental characteristics and performances of different kinds of antenna arrays are listed in Table 5 for comparison.

6 Conclusions

In this study, we have proposed a type of millimeter-wave antenna array with flexible design at 60 GHz. The antenna array can be adjusted to be linearly or circularly polarized by simply changing the radiation part, while the feeding part is kept unchanged. For the 8×8 linearly polarized antenna array, the simulation results show a bandwidth of 21.6%, a gain of (26.1±1) dBi, and antenna efficiency of more

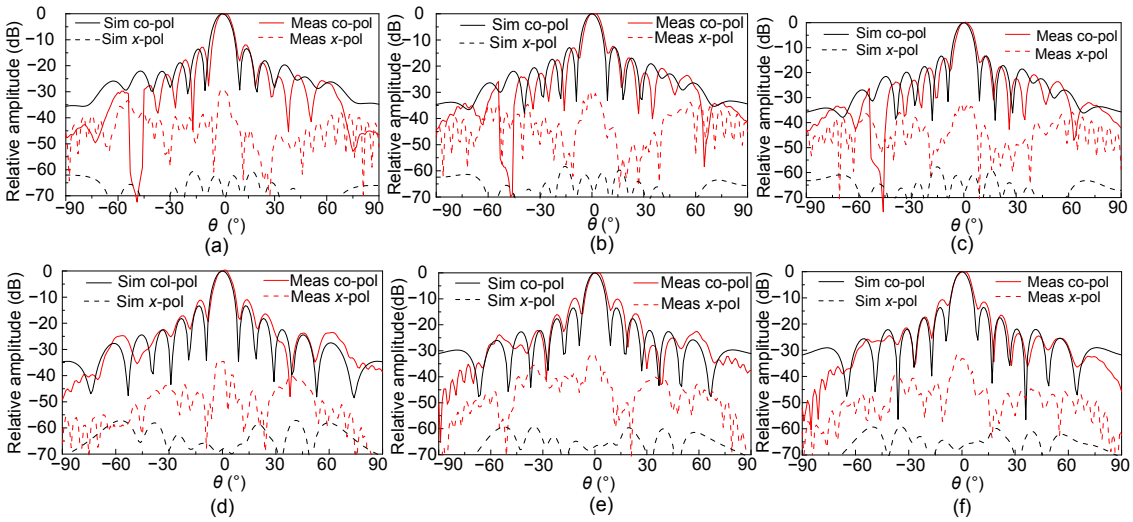

Fig. 34 Simulation and measurement results of the radiation patterns: (a) H-plane, at 60 GHz; (b) H-plane, at 63 GHz; (c) H-plane, at 64 GHz; (d) E-plane, at 60 GHz; (e) E-plane, at 63 GHz; (f) E-plane, at 64 GHz

Sim co-pol: simulated co-polarization; Sim *x*-pol: simulated *x*-polarization; Meas co-pol: measured co-polarization; Meas *x*-pol: measured *x*-polarization

Table 5 Comparison between the proposed antenna array and some antenna arrays in the literature

Reference	Frequency band (GHz)	Impedance bandwidth (%)	3-dB AR bandwidth (%)	Maximum gain (dBi)	Numbers of elements	Maximum efficiency (%)	Fabrication technology
Zhu et al. (2017)	55.0–66.0	18.2	–	20.5	6	44.6	PCB
Li and Luk (2016)	55.0–66.0	18.2	16.5	26.1	64	72.2	PCB
Tomura et al. (2012)	59.0–65.0	11.3	–	32.5	256	83.6	Diffusion bonding
Zarifi et al. (2017)	58.0–67.0	15.5	–	23.0	64	80.0	CNC and PCB
Liu et al. (2017)	54.0–64.0	17.0	–	28.0	256	60.0	CNC and PCB
Liu et al. (2018)	56.5–67.0	17.0	–	27.0	64	85.0	CNC
Ferrando-Rocher et al. (2018)	29.5–31.0	4.0	4.0	22.4	16	90.0	CNC
Akbari et al. (2018)	28.0–35.0	22.0	21.8	23.5	64	85.0	CNC
Irie and Hirokawa (2017)	59.0–63.5	8.0	–	32.7	256	80.0	Diffusion bonding and PCB
Proposed LP	55.0–68.0	21.6	–	26.8	64	86.0	Diffusion bonding and PCB
Proposed CP*	57.0–68.0	18.2	13.3	27.6	64	88.0	Diffusion bonding and PCB

* Simulation results. PCB: printed circuit board; CNC: computer numerical control machine tools. LP: linearly polarized; CP: circularly polarized

than 80% in the bandwidth. For the 8×8 circularly polarized antenna, the simulation results show that the impedance bandwidth of 18.2% and AR bandwidth of 13.3% are obtained. Gain and efficiency of up to 27.6 dBic and 88% are achieved, respectively. A prototype of the linearly polarized antenna array has been fabricated, and the measurement results are in good agreement with the simulation results that a realized gain of more than 23.8 dBi and the measured maximum efficiency of 86% over the band have been obtained. This type of high efficiency antenna array would be a promising candidate for millimeter-wave wireless communication.

Contributors

Kai-lai WU designed the research, conducted the investigation, and wrote the first draft of the manuscript. Yuan YAO, Jun-sheng YU, and Xiao-dong CHEN supervised the research. Yuan YAO, Xiao-he CHENG, and Tao YU helped organize the manuscript. Kai-lai WU and Yuan YAO revised and edited the final version.

Compliance with ethics guidelines

Kai-lai WU, Yuan YAO, Xiao-he CHENG, Jun-sheng YU, Tao YU, and Xiao-dong CHEN declare that they have no conflict of interest.

References

Akbari M, Farahbakhsh A, Sebak AR, 2018. Ridge gap waveguide multilevel sequential feeding network for high-gain circularly polarized array antenna. *IEEE Trans Antenn Propag*, 67(1):251-259. https://doi.org/10.1109/TAP.2018.2878281

Du M, Dong YL, Xu J, et al., 2017. 35-GHz wideband circularly polarized patch array on LTCC. *IEEE Trans Antenn Propag*, 65(6):3235-3240. https://doi.org/10.1109/TAP.2017.2689073

Ferrando-Rocher M, Herranz-Herruzo JI, Valero-Nogueira A, et al., 2018. Single-layer circularly-polarized Ka-band antenna using gap waveguide technology. *IEEE Trans Antenn Propag*, 66(8):3837-3845. https://doi.org/10.1109/TAP.2018.2835639

Hao ZC, Li BW, 2017. Developing wideband planar millimeter-wave array antenna using compact magneto-electric dipoles. *IEEE Antenn Wirel Propag Lett*, 16: 2102-2105. https://doi.org/10.1109/LAWP.2017.2697903

Irie H, Hirokawa J, 2017. Perpendicular-corporate feed in three-layered parallel-plate radiating-slot array. *IEEE Trans Antenn Propag*, 65(11):5829-5836. https://doi.org/10.1109/TAP.2017.2751659

Kildal PS, Alfonso E, Valero-Nogueira A, et al., 2008. Local metamaterial-based waveguides in gaps between parallel metal plates. *IEEE Antenn Wirel Propag Lett*, 8:84-87. https://doi.org/10.1109/LAWP.2008.2011147

Lee B, Yoon Y, 2017. Low-profile, low-cost, broadband millimeter-wave antenna array for high-data-rate WPAN systems. *IEEE Antenn Wirel Propag Lett*, 16:1957-1960. https://doi.org/10.1109/LAWP.2017.2690440

Li YJ, Luk KM, 2016. A 60-GHz wideband circularly polarized aperture-coupled magneto-electric dipole antenna array. *IEEE Trans Antenn Propag*, 64(4):1325-1333. https://doi.org/10.1109/TAP.2016.2537390

Liu JL, Vosoogh A, Zaman AU, et al., 2017. Design and fabrication of a high-gain 60-GHz cavity-backed slot antenna array fed by inverted microstrip gap waveguide. *IEEE Trans Antenn Propag*, 65(4):2117-2122. https://doi.org/10.1109/TAP.2017.2670509

Liu JL, Vosoogh A, Zaman AU, et al., 2018. A slot array antenna with single-layered corporate-feed based on ridge gap waveguide in the 60 GHz band. *IEEE Trans Antenn Propag*, 67(3):1650-1658. https://doi.org/10.1109/TAP.2018.2888730

Miura Y, Hirokawa J, Ando M, et al., 2011. Double-layer full-corporate-feed hollow-waveguide slot array antenna in the 60-GHz band. *IEEE Trans Antenn Propag*, 59(8):2844-2851. https://doi.org/10.1109/TAP.2011.2158784

Parshin VV, Tretyakov MY, Shanin VN, et al., 2001. Modern technique for absorption investigation in atmosphere and condensed media in the MM wavelength range. 4th Int Kharkov Symp on Physics and Engineering of Millimeter and Sub-millimeter Waves, p.79-84. https://doi.org/10.1109/MSMW.2001.946750

Rappaport TS, Murdock JN, Gutierrez F, 2011. State of the art in 60-GHz integrated circuits and systems for wireless communications. *Proc IEEE*, 99(8):1390-1436. https://doi.org/10.1109/JPROC.2011.2143650

Rappaport TS, Sun S, Mayzus R, et al., 2013. Millimeter wave mobile communications for 5G cellular: it will work! *IEEE Access*, 1:335-349. https://doi.org/10.1109/ACCESS.2013.2260813

Tomura T, Miura Y, Zhang M, et al., 2012. A 45° linearly polarized hollow-waveguide corporate-feed slot array antenna in the 60-GHz band. *IEEE Trans Antenn Propag*, 60(8):3640-3646. https://doi.org/10.1109/TAP.2012.2201094

Yamamoto T, Zhang M, Hirokawa J, et al., 2014. Wideband design of a circularly-polarized plate-laminated waveguide slot array antenna. Int Symp on Antennas and Propagation, p.13-14. https://doi.org/10.1109/ISANP.2014.7026486

Zaman AU, Kildal PS, 2016. Gap waveguides. In: Chen Z (Ed.), Handbook of Antenna Technologies. Springer, Singapore, p.3273-3347. https://doi.org/10.1007/978-981-4560-75-7_130-1

Zarifi D, Farahbakhsh A, Zaman AU, et al., 2016. Design and fabrication of a high-gain 60-GHz corrugated slot antenna array with ridge gap waveguide distribution layer. *IEEE Trans Antenn Propag*, 64(7):2905-2913. https://doi.org/10.1109/TAP.2016.2565682

Zarifi D, Farahbakhsh A, Zaman AU, 2017. A gap wave-guide-fed wideband patch antenna array for 60-GHz applications. *IEEE Trans Antenn Propag*, 65(9):4875-4879. https://doi.org/10.1109/TAP.2017.2722866

Zhu JF, Li SF, Liao SW, et al., 2017. High-gain series-fed planar aperture antenna array. *IEEE Antenn Wirel Propag Lett*, 16:2750-2754. https://doi.org/10.1109/LAWP.2017.2744665